Chinese Chemical Letters 32 (2021) 1381–1384

Contents lists available at ScienceDirect

Chinese Chemical Letters

journal homepage: www.elsevier.com/locate/cclet

Communication

An AIE singlet oxygen generation system based on supramolecular strategy

Minzan Zuo[a], Weirui Qian[b], Min Hao[b], Kaiya Wang[a], Xiao-Yu Hu[a,*], Leyong Wang[b]

[a] College of Material Science and Technology, Nanjing University of Aeronautics and Astronautics, Nanjing 211106, China
[b] Key Laboratory of Mesoscopic Chemistry of MOE, School of Chemistry and Chemical Engineering, Nanjing University, Nanjing 210023, China

ARTICLE INFO

Article history:
Received 3 August 2020
Received in revised form 7 September 2020
Accepted 21 September 2020
Available online 22 September 2020

Keywords:
Aggregation-induced emission
Singlet oxygen
Self-assembly
Chemiluminescence
Photocatalysis

ABSTRACT

The design of supramolecular systems with efficient singlet oxygen generation has attracted considerable interests. Herein, an AIE-based singlet oxygen generation system with chemiluminescence properties is reported in aqueous media based on supramolecular host–guest assembly between a water-soluble pillar[5]arene (**WP5**) and an AIE photosensitizer (**TPEDM**). The formed supramolecular nanoparticles exhibit significant singlet oxygen generation ability as well as enhanced fluorescence. In addition, by introducing catalase, this H_2O_2-responsive supramolecular system shows increased $^1O_2$ generation efficiency compared with the blank nanoparticles. An efficient chemiluminescence system can also be achieved by entrapping an energy donor adamantane derivative (**AMPPD**). Moreover, the present system can function as nanoreactors to perform the photooxidation of dopamine to form polydopamine with visible light irradiation. This work provides a new strategy for the construction of $^1O_2$ generation system based on supramolecular nanomaterials, which has potential applications in the fields such as chemiluminescence imaging and controlled photocatalysis.

Singlet oxygen ($^1O_2$), a kind of reactive oxygen species (ROS), has attracted a lot of attention because of its broad applications in photodynamic therapy, sewage treatment, catalytic synthesis and so on [1–5]. $^1O_2$ generation is related to photosensitizer, light source, and molecular oxygen. Upon being irradiated with light, the photosensitizer is excited to the singlet state (S_1), which can further switch to the excited triplet state (T_1) through the gap crossing. Consequently, the energy is transferred to the triplet oxygen, generating reactive oxygen radicals [6–8]. The common photosensitizers include BODIPY derivatives, porphyrin derivatives, and chlorin derivatives [9,10]. Although various photosensitizers have been explored so far, most of them have a severe aggregation-induced quenching effect (ACQ). Due to their rigid planar structures, these dyes tend to aggregate in aqueous solution, resulting the energy consumption in a non-radiative manner [11–13]. Thus designing of novel photosensitizers that can avoid these shortcomings in aqueous phase is urgently needed.

Photosensitizers with aggregation induced emission (AIE) effect have offered a good opportunity to address the aforementioned issues [14,15]. Due to the prohibition of energy dissipation and restriction of intramolecular motion, AIE photosensitizers can avoid the ACQ effect and show highly bright fluorescence in the aggregated state. What is more, by incorporating strong donor/acceptor units into a photosensitizer, the HOMO and LUMO distribution can be separated to decrease the ΔE_{ST} (singlet–triplet energy gap). Therefore, the AIE photosensitizers can show efficient $^1O_2$ generation in the aggregate state [16–18]. Currently, most of the AIE photosensitizer systems are focused on the fluorescence emission. However, the requirement of an external light source hinders their application of deep tissue imaging and treatment [19,20]. Therefore, a highly efficient chemiluminescent system without the requirement for an external light source remains to be improved. Meanwhile, considering that the photobleaching of photosensitizers can make them undergo various side reactions, photostability of the photosensitizers is also a thorny issue to be overcome.

Herein, an AIE-based singlet oxygen system constructed by supramolecular assembly has been reported (Scheme 1). The AIE photosensitizer (**TPEDM**) was used as the guest. **TPEDM** has a typical donor-acceptor (D-A) structure, therefore, it shows efficient $^1O_2$ generation property. Considering **TPEDM** has a quaternary ammonium terminal group, water-soluble pillar[5]arene (**WP5**) was used as a more suitable host molecule. In this case, the strong binding affinity between **WP5** and the quaternary ammonium salt

* Corresponding author.
E-mail address: huxy@nuaa.edu.cn (X.-Y. Hu).

https://doi.org/10.1016/j.cclet.2020.09.033
1001-8417/

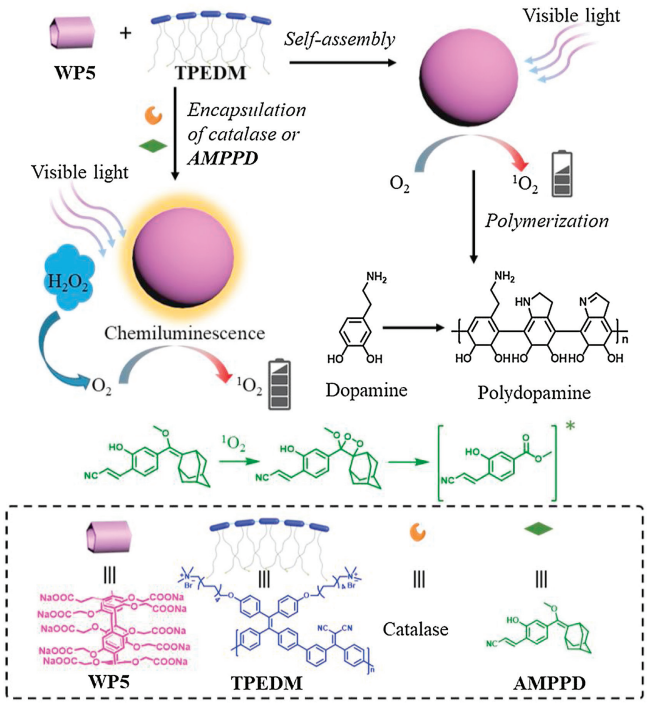

Scheme 1. Schematic illustration of the supramolecular AIE chemiluminescent singlet oxygen generation system.

can induce the formation of stable amphiphilic host-guest complex, which can further self-assemble into supramolecular self-assemblies in aqueous solution. Consequently, supramolecular nanoparticles with efficient $^1O_2$ generation and high fluorescence were achieved. The obtained nanoparticles exhibited excellent photostability. By encapsulation of catalase, the supramolecular system could show increased $^1O_2$ generation efficiency in response to H_2O_2. Upon encapsulating adamantane derivative (**AMPPD**) as an energy donor, a highly efficient chemiluminescence system could be achieved, where the AIE photosensitizer can be excited chemically. Such water-soluble self-luminescent polymeric nanoparticles exhibited high brightness with long-lasting time that could be observed by naked eyes. Moreover, the supramolecular system can function as nanoreactors to perform the photooxidation of dopamine to form polydopamine with visible light irradiation.

As we know, **WP5** can combine with the alkyl quaternary ammonium salts through hydrophobic and electrostatic interaction to form a stable supramolecular complex [21], the self-assembly behavior of **WP5⊃TPEDM** amphiphiles and the formed supramolecular nanostructures were further explored. Firstly, the aggregation behavior of free **TPEDM** was investigated. As shown in Fig. S14 (Supporting information), no Tyndall effect could be observed, suggesting that free **TPEDM** can be well dispersed in water. However, when **WP5** was added into the **TPEDM** solution, notable opalescence as well as obvious Tyndall effect could be clearly observed, indicating that **WP5** can induce the self-assembly behavior of **WP5⊃TPEDM** complex to form highly dispersive nanoparticles [22]. The obtained nanoparticles were quite stable under physiological condition, and the average diameters of nanoparticles did not show obvious change within one week (Fig. S21 in Supporting information). Subsequently, the best molar ratio between **WP5** and **TPEDM** for constructing supramolecular nanoparticles was determined by optical transmittance tests. As shown in Fig. S15 (Supporting information), upon gradually increasing the concentration of **WP5**, the transmittance at 600 nm first underwent a rapid decrease to a minimum and

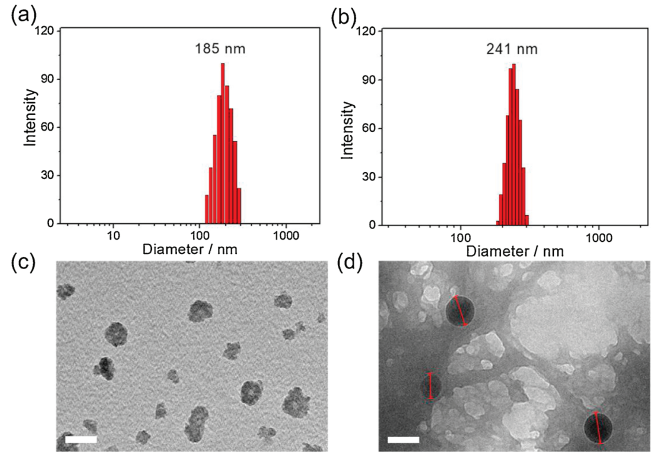

Fig. 1. DLS results of the nanoaggregates formed by **WP5⊃TPEDM** (a) and **AMPPD-WP5⊃TPEDM** (b); TEM images of the **WP5⊃TPEDM** nanoaggregates (c) and **AMPPD-WP5⊃TPEDM** nanoaggregates (d). Scale bar: 200 nm.

thereafter an inverse increase. Thus, the best molar ratio for the formation of supramolecular aggregates was deemed to be 7:1 ([**TPEDM**]/[**WP5**]) at the inflection point. Based on the obtained molar ratio, the critical aggregation concentration (CAC) for **WP5⊃TPEDM** complex was determined to be 1.8×10^{-6} mol/L (Fig. S16 in Supporting information). ζ-Potential assay was also conducted to examine the stability of the **WP5⊃TPEDM** nanoparticles at the best molar ratio. The results showed a negative ζ-potential (–38.5 mV, Fig. S17a in Supporting information) for the formed nanoparticles, indicating that the electrostatic repulsive force is able to prevent nanoparticle agglomeration and improve their stability.

Next, the size distribution and morphology of the **WP5⊃TPEDM** nanoaggregates were determined by dynamic laser scattering (DLS) and transmission electron microscopy (TEM) measurements. DLS data revealed that the **WP5⊃TPEDM** nanoaggregates displayed a narrow size distribution with an average diameter of 185 nm (Fig. 1a). The TEM image (Fig. 1c) indicated the formation of a number of shrunk nanoparticles with diameters around 150 nm.

Given that **TPEDM** is an AIE-based photosensitizer with typical donor-acceptor structure, it may exhibit excellent $^1O_2$ generation efficiency. Thus the $^1O_2$ generation efficiency of the systems was explored. Herein, visible light was used to excite **TPEDM**. As shown in Fig. 2a, nearly 63% 9,10-anthracenediyl-bis(methylene)dimalonic acid (ABDA), a commercially available $^1O_2$ indicator, was consumed for the free **TPEDM** in water at a decomposition rate of 38.7 μmol/min within 100 s of irradiation. When **WP5** was introduced to the system, the decomposition rate of **WP5⊃TPEDM** nanoparticles was determined to be 28.9 μmol/min within 100 s of irradiation. The above phenomenon confirms that both **TPEDM**

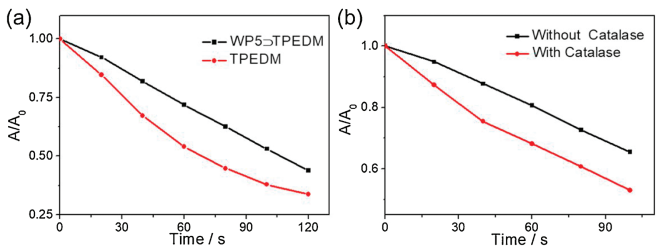

Fig. 2. (a) Singlet oxygen generation efficiency of free **TPEDM** and **WP5⊃TPEDM** nanoparticles ([**WP5**] = 0.5×10^{-4} mol/L, [**TPEDM**] = 0.08 mg/mL, 90 W/m^2 visible light); (b) Singlet oxygen generation efficiency of **WP5⊃TPEDM** nanoparticles with and without the presence of catalase, respectively ([**WP5**] = 0.5×10^{-4} mol/L, [**TPEDM**] = 0.08 mg/mL, 70 W/m^2 visible light).

and **WP5⊃TPEDM** nanoparticles have high $^1O_2$ generation efficiency under visible light irradiation. Moreover, the slightly different $^1O_2$ generation efficiency between free **TPEDM** and **WP5⊃TPEDM** nanoparticles may be due to the fact that **WP5** with electron rich cavity can strongly bind with the **TPEDM** guest, which further influences the donor-acceptor structure of the **TPEDM**, resulting the changes of ΔE_{ST} and $^1O_2$ generation efficiency [23,24]. The $^1O_2$ quantum yield of the **WP5⊃TPEDM** nanoparticles was calculated to be 0.89, using Rose Bengal ($^1O_2$ quantum yield: 0.75) as a reference photosensitizer (Fig. S20 in Supporting information).

In addition, the absorption band at 420–500 nm of the formed nanoparticles has no obvious change after prolonged irradiation (Fig. S18a in Supporting information), indicating that the nanoparticles have good stability and will not undergo photobleaching [25]. To further improve the $^1O_2$ generation efficiency, catalase was used for fabricating H_2O_2-responsive nanoparticles. Catalase can catalyze the decomposition of hydrogen peroxide to produce oxygen, which can be used as the source of oxygen for the system and increase the generation efficiency of $^1O_2$. As was expected, the $^1O_2$ generation of the catalase-**WP5⊃TPEDM** system was significantly improved, and the ABDA decomposition rate was 1.5 times higher than that of the **WP5⊃TPEDM** nanoparticles within 100 s of irradiation (Fig. 2b).

Chemiluminescence has many advantages over fluorescence in imaging, due to its unnecessity of external light sources and high sensitivity. Thus, in order to construct a supramolecular chemiluminescent nanosystem, we further encapsulated a suitable energy donor, adamantane derivative, in the empty nanoparticles. The loaded **AMPPD** can react with singlet oxygen to produce extremely unstable intermediate, which tend to slowly decompose and release energy at room temperature to achieve chemiluminescence [26,27]. Therefore, when the **AMPPD**-loaded nanoparticles were irradiated with visible light, effective chemiluminescence could be observed by naked eye. The size distribution and morphology of the **AMPPD-WP5⊃TPEDM** nanoaggregates were also investigated. As shown in Fig. 1b, **AMPPD-WP5⊃TPEDM** nanoaggregates displayed a narrow size distribution with an average diameter of 241 nm. The TEM image further demonstrated the formation of circular nanoparticles with sizes around 200 nm (Fig. 1d). Next, the fluorescence characteristics of the above system were investigated. Since the free **TPEDM** present dispersed state, the molecules can vibrate freely and the energy is dissipated in a non-radiative manner, therefore, no obvious fluorescence could be observed (Fig. S14). However, when **WP5** was added, the **WP5⊃TPEDM** in aggregation state could prohibit the nonradiative transition and aggregation-induced intersystem crossing, leading to the enhanced fluorescence intensity. Moreover, when **AMPPD** was encapsulated, significant fluorescence could be found for the **AMPPD-WP5⊃TPEDM** system. This may contribute to Förster resonant energy transfer (FRET) from **AMPPD** to **TPEDM**.

We further conducted the study on its UV and fluorescence properties in order to verify the above speculation. The results showed (Fig. 3a) that the fluorescence emission band of **AMPPD** (from 400 nm to 600 nm) is partially overlapped with the UV absorption band of **WP5⊃TPEDM** (from 300 nm to 600 nm). Besides, since **AMPPD** was encapsulated into the nanoparticles, the confined distance between **AMPPD** and the **WP5⊃TPEDM** complex is close enough to ensure the efficient FRET process. Moreover, compared with the **WP5⊃TPEDM** system, the emission band of **AMPPD** at 490 nm in the **AMPPD-WP5⊃TPEDM** system is relatively weak, while the emission band of **TPEDM** at 590 nm is greatly enhanced, indicating that the energy of **AMPPD** may be transferred to **TPEDM** (Fig. 3b). This phenomenon further indicated the FRET process from **AMPPD** to **TPEDM**, resulting in a significant increase in the fluorescence. When the nanoparticles were irradiated with visible light for 5 min, significant

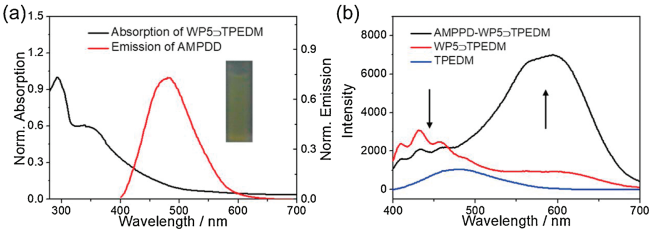

Fig. 3. (a) UV absorption spectra of **WP5⊃TPEDM** nanoparticles and fluorescence spectra **AMPPD**. Inset: Chemiluminescent image of **AMPPD-WP5⊃TPEDM** nanoparticles after the irradiation with xenon lamp for 5 min ([**WP5**] = 0.5×10^{-4} mol/L, [**TPEDM**] = 0.08 mg/mL, [**AMPPD**] = 0.02 mg/mL); (b) Fluorescence spectra **TPEDM**, **WP5⊃TPEDM** nanoparticles, and **AMPPD-WP5⊃TPEDM** nanoparticles ([**WP5**] = 0.5×10^{-4} mol/L, [**TPEDM**] = 0.08 mg/mL, [**AMPPD**] = 0.02 mg/mL).

chemiluminescence could be observed by naked eye, and the chemiluminescence fluorescence could be kept for several minutes.

Considering the excellent $^1O_2$ generation efficiency of the nanoassemblies, we further investigated the possibility of the nanoplatform as nanoreactors. It was dated that the $^1O_2$ can oxidize dopamine to polydopamine, a multifunctional polymer which has strong adhesive property and outstanding photothermal conversion efficiency [28,29]. Therefore, dopamine was chosen as the substrate to demonstrate the photooxidation properties of the nanoassemblies (Fig. 4a). Since the **WP5⊃TPEDM** nanoparticles have larger surface area compared with free **TPEDM** solution, they can adsorb dopamine to promote the catalytic effect. Therefore, **WP5⊃TPEDM** nanoparticles were chosen as nanoreactors for the photooxidation process. The results depicted in Fig. 4b showed that absorbance of the polydopamine solution only increased upon the light irradiation (For details, see Fig. S19 in Supporting information), while the absorbance showed no significant changes without light irradiation. This phenomenon may contribute to the short half-life of $^1O_2$, which is convenient for controlling the polymerization process by regulating the "On/Off" mode of the light irradiation. Because the formed polydopamine may adhere to the surface of the nanoparticles, this smart $^1O_2$ generation system would provide a new insight into fabrication of novel photothermal/photodynamic system.

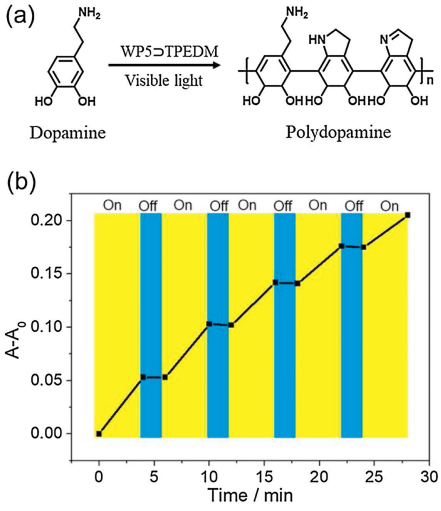

Fig. 4. (a) Schematic illustration of dopamine photooxidation catalyzed by **WP5⊃TPEDM** nanoparticles upon light irradiation. (b) Absorbance changes at 480 nm of the dopamine solution in the presence of **WP5⊃TPEDM** nanoparticles upon light irradiation as a function of time ([**WP5**] = 0.5×10^{-4} mol/L, [**TPEDM**] =0.08 mg/mL, 90 W/m^2 visible light).

In summary, an AIE-based singlet oxygen system has been successfully exploited based on the supramolecular self-assembly between **WP5** and **TPEDM**. In this system, the tetrastyrene conjugated polymer with a donor–acceptor structure exhibited excellent photostability as well as the ability to produce singlet oxygen under visible light irradiation. The fabricated **WP5⊃TPEDM** nanoparticles showed similar singlet oxygen generation efficiency with enhanced fluorescence intensity. By introducing catalase, the self-oxygen supply environment can be provided and a significant increase in the singlet oxygen yield can be achieved compared with the blank nanoparticles. Moreover, an efficient chemiluminescent supramolecular system was constructed by entrapping a suitable energy donor **AMPPD**, which leads to the FRET induced fluorescence and chemiluminescence. Additionally, the present nanoparticles can function as nanoreactors to promote the photooxidation of dopamine to form polydopamine by regulating the "On/Off" mode of the light irradiation. This work provides a new strategy for the construction of $^1O_2$ generation system based on supramolecular nanomaterials, as well as potential application value for chemiluminescence imaging and controlled photocatalysis.

Declaration of competing interest

The authors report no declarations of interest.

Acknowledgments

This work was supported by the National Natural Science Foundation of China (No. 21871136), the Natural Science Foundation of Jiangsu Province (No. BK20180055), and the Fundamental Research Funds for the Central Universities (No. NE2019002).

Appendix A. Supplementary data

Supplementary material related to this article can be found, in the online version, at doi:https://doi.org/10.1016/j.cclet.2020.09.033.

References

[1] A.A. Ghogare, A. Greer, Chem. Rev. 116 (2016) 9994–10034.
[2] K. Yang, J. Wen, S. Chao, et al., Chem. Commun. 54 (2018) 5911–5914.
[3] Z. Liu, J. Wu, C. Wang, et al., Chin. Chem. Lett. 30 (2019) 2299–2303.
[4] L.L. Rui, H.L. Cao, Y.D. Xue, et al., Chin. Chem. Lett. 27 (2016) 1412–1420.
[5] J. Han, K. Liu, R. Chang, L. Zhao, X. Yan, Angew. Chem. Int. Ed. 58 (2019) 2000–2004.
[6] J. Zhao, W. Wu, J. Sun, S. Guo, Chem. Soc. Rev. 42 (2013) 5323–5351.
[7] J. Veerman, M. Garcia-Parajo, L. Kuipers, N. Van Hulst, Phys. Rev. Lett. 83 (1999) 2155–2158.
[8] C.A. Robertson, D.H. Evans, H. Abrahamse, J. Photochem. Photobiol. B 96 (2009) 1–8.
[9] A. Kamkaew, S.H. Lim, H.B. Lee, et al., Chem. Soc. Rev. 42 (2013) 77–88.
[10] C.K. Prier, D.A. Rankic, D.W. MacMillan, Chem. Rev. 113 (2013) 5322–5363.
[11] F. Hu, S. Xu, B. Liu, Adv. Mater. 30 (2018) 1801350.
[12] D. Wang, H. Su, R.T.K. Kwok, Chem. Sci. 9 (2018) 3685–3693.
[13] N. Jiang, Y. Wang, A. Qin, J. Sun, B. Tang, Chin. Chem. Lett. 30 (2019) 143–148.
[14] P. Wang, X. Yan, F. Huang, Chem. Commun. 50 (2014) 5017–5019.
[15] L. Shao, J. Sun, B. Hua, F. Huang, Chem. Commun. 54 (2018) 4866–4869.
[16] W. Qian, M. Zuo, G. Sun, et al., Chem. Commun. 56 (2020) 7301–7304.
[17] E. Zhao, Y. Chen, H. Wang, et al., ACS Appl. Mater. Interfaces 7 (2015) 7180–7188.
[18] L. Yang, X. Wang, G. Zhang, et al., Nanoscale 8 (2016) 17422–17426.
[19] Y. Gao, Y. Lin, T. Liu, et al., Chin. Chem. Lett. 30 (2019) 63–66.
[20] J. Cao, J. Campbell, L. Liu, R.P. Mason, A.R. Lippert, Anal. Chem. 88 (2016) 4995–5002.
[21] M. Zuo, W. Qian, Z. Xu, et al., Small 14 (2018) 1801942.
[22] A.L. Koner, W.M. Nau, Supramol. Chem. 19 (2007) 55–66.
[23] C. Chen, X. Ni, H.W. Tian, et al., Angew. Chem. Int. Ed. 59 (2020) 10008–10012.
[24] L. Shao, Y. Pan, B. Hua, et al., Angew. Chem. Int. Ed. 59 (2020) 11779–11783.
[25] W. Wu, D. Mao, S. Xu, et al., Chem 4 (2018) 1937–1951.
[26] O. Green, T. Eilon, N. Hananya, et al., ACS Cent. Sci. 3 (2017) 349–358.
[27] S. Gnaim, D. Shabat, Chem 139 (2017) 10002–10008.
[28] X. Du, L. Li, J. Li, et al., Adv. Mater. 26 (2014) 8029–8033.
[29] W. Cheng, X. Zeng, H. Chen, et al., ACS Nano 13 (2019) 8537–8565.